**Journal of Ceramic Science and Technology**

# Interlaminar Shear Response of Carbon/Carbon in Torsion Tests

## T. Krause[1], R.S.M. Almeida[2], E. Volkmann[3], K. Tushtev[*2], D. Koch[4], K. Rezwan[2, 5], G. Grathwohl[2]

[1]Airbus Operations GmbH, D-21129 Hamburg, Germany.
[2]Advanced Ceramics, University of Bremen, D-28359 Bremen, Germany.
[3]OHB System AG, D-28359 Bremen, Germany.
[4]Institute of Structures and Design, German Aerospace Center, D-70569 Stuttgart, Germany.
[5]MAPEX - Center for Materials and Processes, University of Bremen, D-28359 Bremen, Germany.

## Abstract

Ceramic matrix composites offer remarkable strength and toughness and are usually designed based on the stacking of fiber plies. These composites are susceptible to debonding of these plies, as their interlaminar strength is significantly lower than in direction of the fibers. In this study, the application of torsion tests for the measurement of the interlaminar shear strength was evaluated using carbon/carbon composites with different porosities. Results obtained with the proposed technique are in accordance with standard methods such as short-beam flexure or double-notched compression. In contrast to these other methods, the torsion test also allows accurate control of superimposed normal stresses on the designated shear plane. The response of the composite samples in loading situations with variable ratios of shear and normal stresses could then be evaluated, leading to failure envelope curves. Different interlaminar fracture mechanisms were discovered depending on the level of normal stress.

*Keywords: Carbon fibers, ceramic matrix composites (CMCs), delamination, shear strength.*

## I. Introduction

Carbon/carbon composites (C/C) and other ceramic matrix composites (CMC) are used increasingly in industrial applications. Originally developed for the aerospace industry, extensive research over the past three decades has widened the field of application to refractories and motorsports. The main advantage of such materials is their combination of high strength and considerable toughness. This mechanical behavior is associated with several toughening mechanisms achieved by either a weak matrix or weak fiber/matrix interface or a combination of both. In contrast to the high in-plane strength, these composites tend to exhibit a much lower interlaminar strength. Therefore, application limits are often indicated by the interlaminar failure of CMC, which eventually results in the debonding of the individual fiber plies and subsequent failure of the entire component.

Several test methods are used in CMC research to evaluate interlaminar strength, albeit almost all articles use only one of them to characterize a particular material. The most common method is the flexural test with a short distance span width of the lower support (short-beam bending, SBB) [1]. Owing to its simplicity, the three- or four-point SBB test is widely used for quality monitoring and the evaluation of new material developments. The interlaminar shear strength is computed under the assumption of a parabolic shear stress distribution over the cross-section of the specimen, cf. ASTM D2344. However, CMCs can offer a wide range of responses to flexural loading, starting from SiC/SiC materials with very strong layer-interfaces to some oxide/oxide and carbon/carbon composites with a highly porous interlayer matrix. For instance, a denser matrix was reported to enhance brittle behavior in SBB tests of carbon/carbon composites [2]. Moreover, it is well known that the loading and support rolls cause indentation deformation and local compressive stresses which usually result in an overestimation of the interlaminar shear strength.

An alternative method is the double-notched compression test (DNC, ASTM D3846) [3]. It was designed to set up a state of pure shear in the middle plane of the composite specimen, thus being unaffected by other stresses. However, it was proven by means of finite element analysis that stress concentrations can arise from the notches [4]. The notch distance must neither be too large nor to small, as both cases result in apparently higher values of the shear strength [5]. In comparison to SBB, results from the DNC test are more conservative. The effect of highly concentrated stresses around notches offers an explanation for shear strengths that are lower than from the SBB test [6]. However, DNC is preferable if the matrix layer connecting the ceramic fiber plies is considerably weaker and thus less stiff.

Another option is the Iosipescu test, in which stress concentration can be controlled by the structure of the notches (ASTM D5379). Still, the application of this test

* Corresponding author: tushtev@uni-bremen.de

is not trivial because of the limited thickness of the C/C plates [7]. Shi *et al.* were able to measure mechanical properties of a short-fiber C/SiC ceramic [8]. Additionally, shear stress distributions of all afore-mentioned methods consider isotropic materials, which is not the case with CMCs, but it is generally assumed that the indicated stress distributions are also applicable for such materials.

The only interlaminar test able to control the amount of superimposed normal and shear stresses applicable to CMCs is the slant shear test. It uses rectangular specimens which are tested in a uniaxial testing device, but under a certain angle from the neutral plane (ASTM C882). Using this technique, Hahn *et al.* assumed a linear relation between the compression load and the shear stress [9]. However, the slant shear test is rarely used for the characterization of CMCs, presumably due to the effort of arranging several angular supports to obtain different ratios of normal/shear stresses. Besides, combined shear/tension tests are difficult to perform with this method owing to the sensitive behavior of CMCs under out-of-plane tension [5].

The Arcan test [10, 11] is used for the measurement of in-plane properties of polymer composites and concrete. A sin-cos relation of normal and shear loads is used to characterize the materials. This comes out as a drawback when the interlaminar load response of heterogeneous materials like C/C (weak matrix, densified fiber plies) is to be evaluated.

Torsion is another method for the application of pure shear stresses and is preferably used in tests of laminated tubes. Recent studies proved that torsion tests are also suitable for the measurement of shear strength of polymer joints [12–14] and glass sealants [15]. Sample preparation for this kind of test is relatively simple and the amount of material needed is small. In addition, a combination of the generated shear stresses with normal stresses is easy to realize [16, 17] compared to common multiaxial test methods [18]. For CMCs, studies of superimposed normal and shear stresses are rare and have mainly been regarded in respect of the so-called in-plane properties, that is in the same plane as the fiber arrangement [19, 20]. In the literature, multiaxial tests are normally performed using thin-walled tubular specimens [21, 22]. However, studies on out-of-plane loadings are very important, since small superimposed tensile stresses can drastically reduce the interlaminar strength [5].

Given that the above-mentioned limitations regarding the superposition of interlaminar loads as well as application to heterogeneous materials, the present paper presents a new test method for interlaminar shear strength measurement based on the application of torsional moments. To validate this method, pure shear results of a carbon/carbon composite were compared to the standard methods SBB and DNC. In addition, the setup proposed enables easy control of superimposed normal stresses what is not possible in SBB and DNC. Thus, the effect of combined normal and shear stresses on the interlaminar fracture strength of this composite was also analyzed.

## II. Experimental

### (1) Materials

A carbon/carbon composite based on a 20-plies lay-up of 2 – 2 twill weave was supplied by Schunk Kohlenstofftechnik, Heuchelheim/Germany. The fiber bundles contained 6000 HT-carbon fibers. The matrix was built up by means of liquid polymer infiltration (LPI) of phenolic resin, followed by thermal processing at maximum temperatures of 2 000 °C. To evaluate the torsion method proposed, two types of this material were used. The first with only one processing cycle and the second with three infiltrations, resulting in an open porosity of 19 % and 8 %, respectively. Fig. 1 shows scanning electron microscopy (SEM) images of the two materials. After three infiltration cycles, many of the original vertical shrinkage cracks inside the fiber bundles are diminished and the inter-ply interface is also further densified, as voids between 0° and 90° fibers are closed. The matrix itself is glassy and shows segmentation effects induced by the shrinkage cracks during curing of the material.
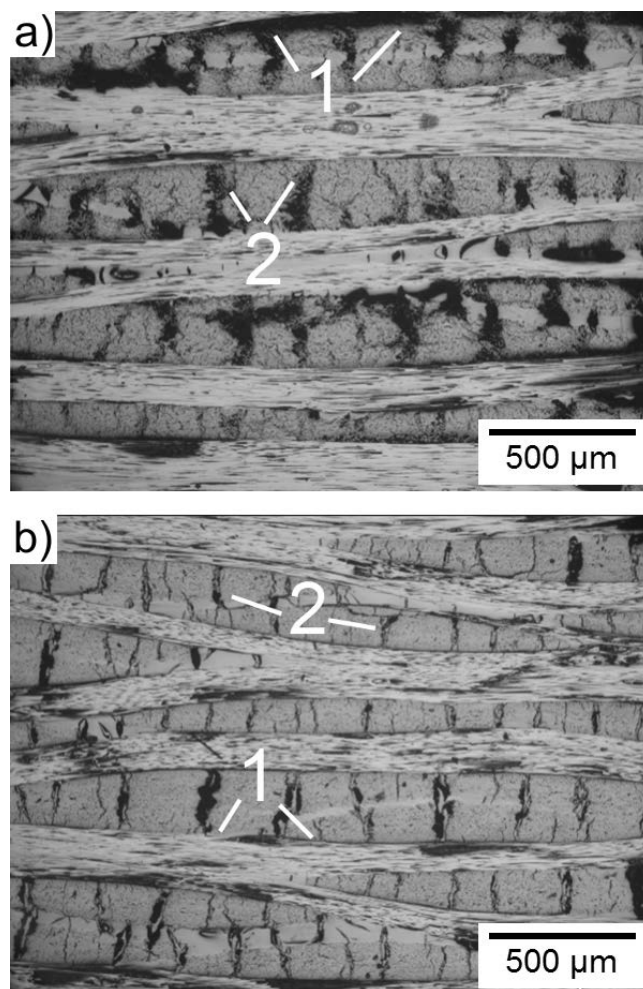


**Fig. 1:** Cross-sections of carbon/carbon composites subjected to one (a) and three (b) matrix infiltration cycles. Interfacial voids (1) and shrinkage cracks (2) are reduced by the additional infiltration cycles.

### (2) Torsion tests

For the torsion tests, specimens were cut from the composite plates (thickness $h = 6.7 \pm 0.1$ mm) using a water-

cooled diamond disk cutter (Cuto, Jean-Wirtz GmbH, Düsseldorf/Germany). All samples had a square base section with an edge length $d_{tor} = 10 \pm 0.1$ mm. A circular cross-section in the middle was prepared by introducing a circumferential notch. This circular part of the sample was chosen as it provides a steady stress at the outer perimeter of this specimen section. The preparation of the reduced circular section was performed using a wire drum saw (Well® 6234, Well Diamond Wire Saws S A, Le Locle/Switzerland) with a diamond-coated wire of 0.5 mm diameter. The resulting section had a diameter $2r = 8 \pm 0.2$ mm (Fig. 2a), which was controlled by means of optical microscopy after the test.

Tests were carried out using a universal test machine Z005 from Zwick GmbH & Co. KG, Ulm/Germany. A 5 kN Zwick/Roell XforceP load cell was used to measure the axial forces, and the torque was measured with a 20 Nm Zwick/Roell Serie M load cell. Twist angles were recorded by the inherent sensor of the machine at the upper part of the load line. Thus, the total twist of the overall setup was recorded. The setup engineered for the torsion shear tests is depicted in Fig. 2. Two fixtures were machined to support the upper and the lower part of the torsion sample. A groove for the specimens to be positioned with a depth of 1.5 mm and a width of $10 \pm 0.1$ mm was machined, cf. Fig. 2b. The fixtures were aligned so that both grooves would face the same direction. Specimens were positioned in the middle of the fixtures with the aid of a caliper. The upper fixture was then moved further downwards until the preselected contact force was reached.
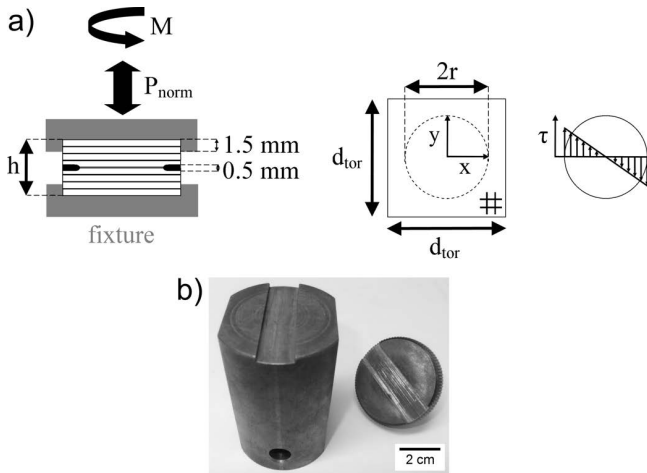


**Fig. 2:** Schematic of test configuration and specimen dimensions showing the reduced cross-section (a). Specimen fixtures used for the torsion tests (b).

Torsion tests were performed at constant speed of 1 °/min and with different levels of superimposed axial forces. All normal stresses were pre-applied before the test with a displacement rate of 0.5 mm/min. A few tests were performed applying both torsion and normal loads at the same time, but the results were in the same range as the tests with pre-applied normal stress. Samples tested with tensile and zero normal stresses were glued to the fixture using epoxy resin (UHU® Plus Schnellfest, UHU GmbH, Buehl/Germany) and the machine was set to hold the desired level of stress. During the curing time of 30 min, the steel pins were fixed in the testing machine in manual load-control mode

at 20 – 30 N of compression and slightly twisted at a fixed torsion moment of 0.1 Nm. This was done in order to ensure that the specimen would be in contact with the edges of the machined grooves. Through-thickness tensile tests, without torsional loads, were carried out in the same setup at a loading rate of 0.5 mm/min using square specimens with an edge length of $10 \pm 0.1$ mm.

For all test methods covering the interlaminar shear strength $\tau_{tor}$, it is assumed that failure occurs in the part of the specimen where the shear stress reaches its maximum. The shear stress $\tau$ at a given point of a circular specimen cross-section can be calculated with:

$$\tau = \frac{M}{I_p}\rho \qquad (1)$$

where $M$ is the applied torsion moment, $I_p$ is the polar second moment of area, and $\rho$ is the radial distance to the given point. For the specimen type presented in this study, the maximum shear stress at a given moment $M$ occurs at the outer perimeter of the reduced circular cross-section. In other words, when $\rho$ is equal to $r$:

$$\tau_{tor} = \frac{2M}{\pi r^2} \qquad (2)$$

The applied normal stress $\sigma$ was calculated using the normal force $P_{norm}$:

$$\sigma = \frac{P_{norm}}{\pi r^2} \qquad (3)$$

### (3) Short-beam bending tests

Four-point bending tests were performed according to DIN EN 658 – 5, using the same machine from the torsion tests. An HBM U2B load cell from HBM Messtechnik, Darmstadt, Germany, with a capacity of 5 kN was used to record the reaction force. The inner support distance $l_{SBB}$ was 20 mm and the outer support distance $L_{SBB}$ was 50 mm. Support rolls had a diameter of 10 mm and specimens had a width $b_{SBB}$ of $10 \pm 0.5$ mm. Fibers were oriented in 0°/90° to width and length of the specimen. Tests were performed in displacement rate control mode at 0.5 mm/min. Shear strength was then calculated using the maximum force $P_{max}$ by

$$\tau_{SBB} = \frac{3P_{max}}{4b_{SBB}h} \qquad (4)$$

### (4) Double-notched compression tests

DNC tests were performed in accordance with DIN EN 658 – 4. The same machine as for torsion tests and bending tests was used. Specimens had a length of 28 mm and a width $b_{DNC}$ of 10 mm. Two notches were machined using a diamond-wire drum saw. The notches had a depth of $h/2 + 0.1$ mm, thus overlapping in the middle. The notch distance $d_{notch}$ was $8.0 \pm 0.5$ mm and the loading rate was set to 0.5 mm/min. Fibers were oriented in 0°/90° to the width and length of the specimen. Specimens were laterally supported in the test rig to prevent kinking.

Shear strength was calculated according to DIN EN 658 – 4 from the maximum force $P_{max}$:

$$\tau_{DNC} = \frac{P_{max}}{b_{DNC}d_{notch}} \qquad (5)$$

## III. Results

### (1)  SBB and DNC results

SBB samples presented a linear load response at the beginning of the test, followed by a non-linear part close to the maximum stress. Afterwards, the load decreased slowly and no sharp load drop was detected. Shear strength $\tau_{SBB}$ was calculated as 7.5 ± 0.3 MPa for specimens with one matrix infiltration and increased to 11.9 ± 0.3 MPa for three infiltrations, although the failure pattern did not completely comply with the requirements to determine the shear strength with Eq. 4. Specimens did not show single large-scale delamination in the middle plane, but multiple smaller delaminations in several of the planes around the lower supports. Investigations of the crack path by means of SEM showed debonding of fibers from the surrounding carbon matrix as the driver of crack propagation.

In contrast, DNC samples presented a linear behavior until the maximum load, followed by a sharp load drop. Shear strength $\tau_{DNC}$ was 5.5 ± 1.8 MPa and 8.0 ± 1.4 MPa for one and three infiltrations, respectively. Similar to SBB, fractography showed progressive fiber-matrix debonding between the plies as the cause for failure.

### (2)  Pure shear torsion tests

Fig. 3 presents exemplary curves of torsion tests without normal stresses. Four different parts (1) – (4) in the stress-twist plots were identified. At first, the test curves showed a small linear onset with a higher slope until about 0.1° (1), which was then followed by a slight decrease in slope (2). Before the maximum shear stress was reached, a further decreasing slope similar to the SBB test could be observed, which was accompanied by small load drops (3). After passing the maximum, the load dropped stepwise, implying progressive failure (4). All specimens with zero normal force did not fall apart during testing, despite being twisted further after the maximum load was reached. Maximum shear stress $\tau_{tor}$ was 6.0 ± 0.4 MPa for one infiltration and 11.7 ± 0.5 MPa for three infiltrations.
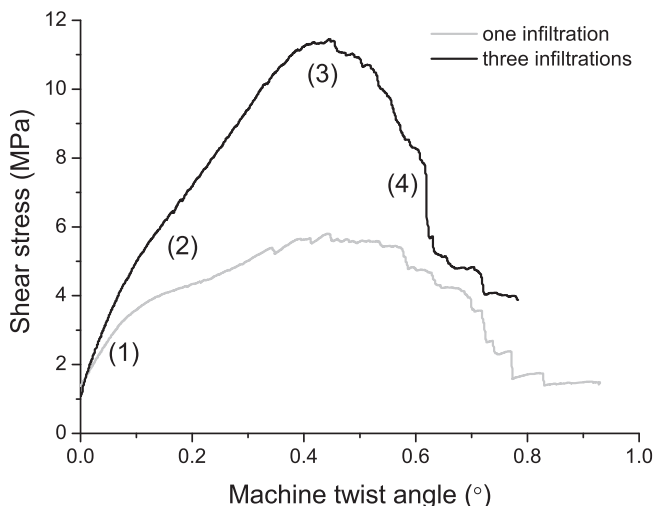
**Fig. 3:** Stress-twist plots of carbon/carbon composites with one and three matrix infiltrations without superimposed axial stress; four distinct regions are highlighted.

### (3)  Torsion tests with superimposed normal stresses

The mechanical behavior of the samples tested with superimposed forces showed a distinct relation to the level of normal stress applied. Fig. 4 shows examples of stress-twist plots of three infiltration specimens tested with and without normal stresses. It should be noted that the overall twist of the set-up was used for the plots. Therefore, it is not possible to make a quantitative comparison of the curves inclination. Still, a clear change in the curve shape can be perceived. Samples tested with tensile loads presented a similar pre-failure curve compared to zero normal stresses, though a much more significant change in slope was observed in the second part of the test curve. This sudden change of slope indicates delamination prior to the total failure of the material. More differences were seen in the post-failure behavior. The torsional moment dropped rapidly when the maximal load was reached. As previously discussed, the pre-defined axial force was kept on the same level by the machine until specimen failure. Once the continuously increasing torque is applied, crack growth is promoted. This additional damage led to rapid specimen failure due to the response of the machine to the crack-initiated decrease of the normal force.
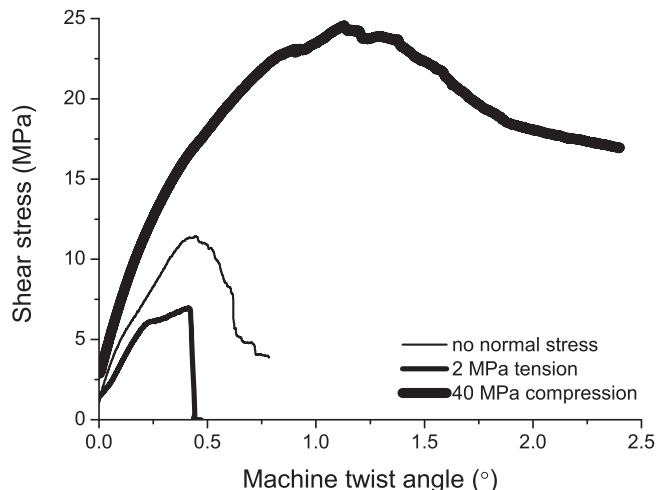
**Fig. 4:** Plots for superimposed tensile and compressive stresses on shear stresses for samples with three infiltrations samples. Note that specimens with normal tensile stress were glued to the fixture affecting the shape of the curve in contrast to compression tests.

The torque-twist plots for superimposed compressive stresses showed two characteristics depending on the compressive stress level. The sudden change of slope in the torque-twist plots was less intense and visible only for specimens below $\sigma$ = -5 MPa. Above this level, the shape of the plot changed to be more continuous with a constantly decreasing slope for further twist. The post-failure behavior was also influenced by the normal loads. For higher compression, the load drops after the maximum were reduced in size. At axial stresses exceeding -38/-43 MPa (one/three infiltrations), these drops almost disappeared even though the specimen had visibly failed. Experiments were then not carried out with axial stresses higher than -44 MPa.

Fig. 5 summarizes the shear and normal stresses at fracture for all torsion tests in a joint plot. The observed fracture patterns as indicated in the figure are discussed in the following sections. The maximum shear stresses decreased rapidly for very small increases of the tensile load. For instance, at tensile stresses of 0.5 MPa, the maximum shear stress decreased to 4.7 MPa (-22 % compared to zero normal stress) and 10.8 MPa (-8 %) for one and three infiltrations, respectively. Maximum tensile stresses that could be achieved were 0.7 MPa for one infiltration and 2.2 MPa for three infiltrations, as after this point, samples failed initially before the application of torsion moments. The pure tensile tests revealed a through-thickness tensile strength of 1 ± 0.1 MPa and 2 ± 0.2 MPa for one and three infiltrations, respectively, which goes well with the highest applicable tensile stresses in the torsion tests. With the application of superimposed compression loads, the fracture shear stress increased. This increase was non-linear, being steeper for relative low compressive loads. The maximum shear stresses measured were about 28 MPa at compressive stresses of -33 MPa for three matrix infiltrations. For one matrix infiltration, this maximum was about 15 MPa at around -25 MPa of compression. Further rise of the compressive force led to a decrease of the shear stress at the point of failure. The overall plot is a failure envelope similar to those calculated for in-plane properties of composites.
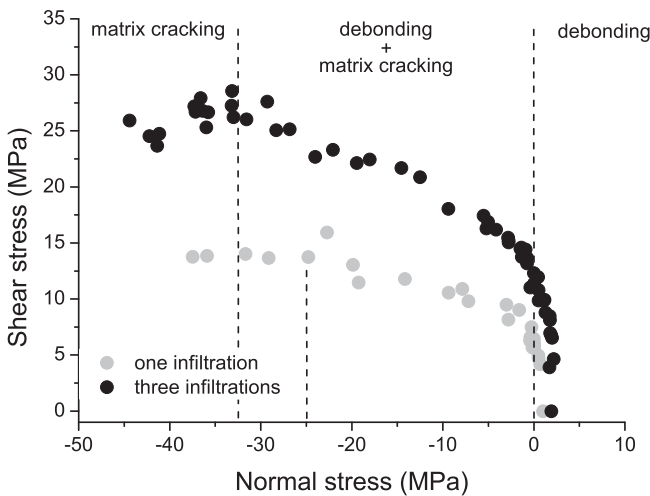


**Fig. 5:** Overall normal stress vs. shear stress at fracture for both C/C with one and three infiltrations.

## (4) Fractography

All torsion specimens failed in the central round area (Fig. 6a). It is then presumed that the failure initiated at cracks close to the outer perimeter of the cross-section due to the higher shear stress. Exposed fibers and fiber imprints were found for both materials as seen in Fig. 6b. The failure occurred at the interfaces of two fiber plies, between the matrix layers and the neighboring 0° or 90° fibers, and was rather straight from one end of the reduced section to the other (cf. Fig. 7a). Specimens with overlaying tensile forces presented similar fracture patterns, but more damage on the fiber plies was observed. In some cases, the cracks were not confined to only one interface, but were also able to cross a fiber bundle and continue growth
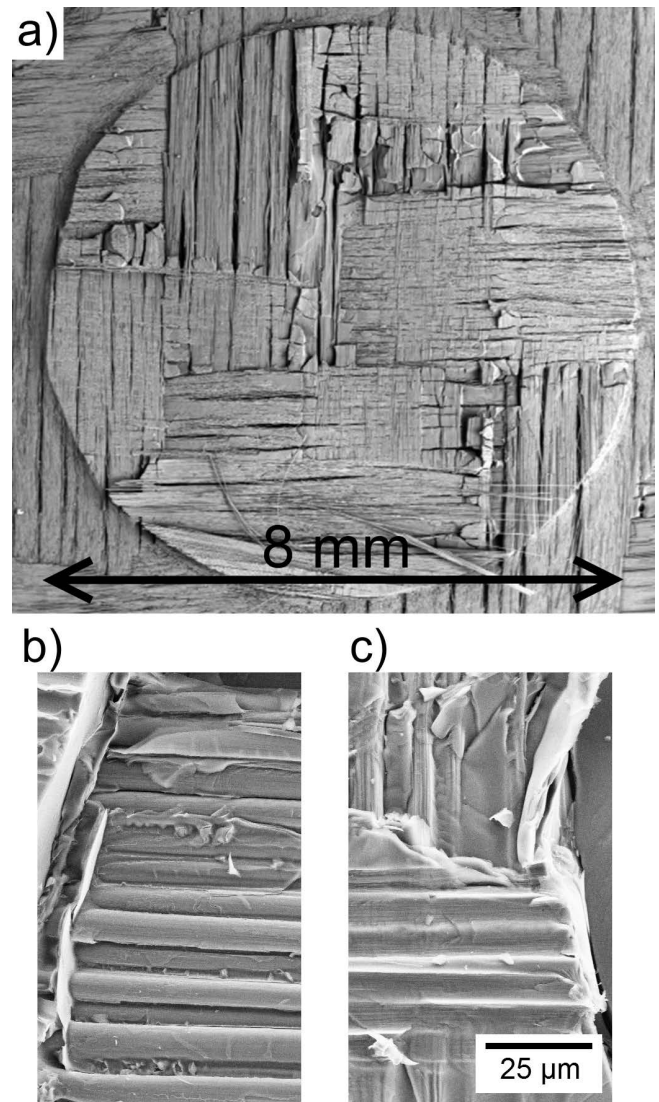


**Fig. 6:** Fracture surface of a torsion specimen with one matrix infiltration which was further twisted after the maximum stress was reached (a). Debonded fibers (b) and matrix imprints (c) at a specimen with three infiltrations. This debonding process was the main fracture mechanism observed for both materials loaded by small superimposed tensile and compressive stresses.
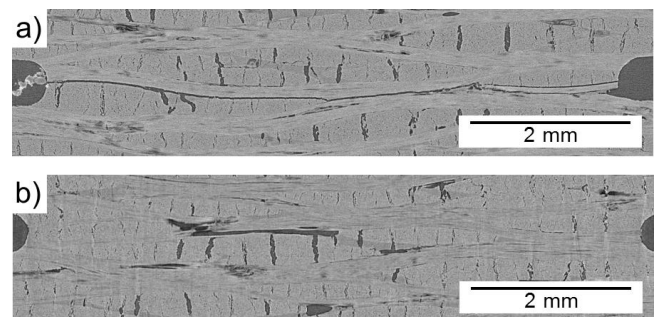


**Fig. 7:** Tomography pictures from torsion specimens failed at normal stresses of (a) -1 MPa and (b) -5 MPa revealing (a) wide-spread and (b) localized delaminations.

at its opposite interface. Sometimes, this led to two cracks growing at both interfaces.

For increasing compressive loads, the formation of large interlaminar cracks in the reduced cross-section was diminished. Although several small delaminations were vis-

ible, they did not instantly spread throughout the entire specimen (Fig. 7b). Under compressive stresses close to and beyond the maximum normal stress at -33 MPa (cf. Fig. 5) the matrix layer was mostly destroyed after the tests. Fig. 8 illustrates that carbon matrix fragments covered the fracture surface and that the fiber imprints were partially sheared off at their exposed parts.
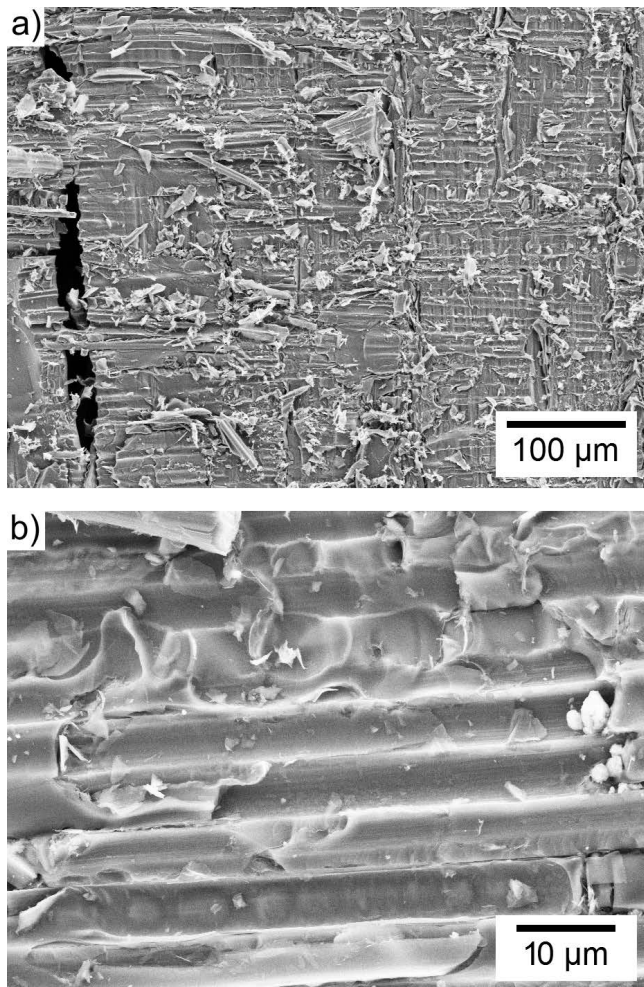


**Fig. 8:** Fracture surface of specimen with three matrix infiltrations and a compressive stress of -35 MPa. Several matrix fragments were dispersed over the fracture surface (a) and fiber imprints were sheared off (b) during the torsion test.

## IV. Discussion

### (1) Shear strength tests

Torsion tests could be successfully used to measure the shear strength of different C/C composites under a state of pure shear stress. During the test, different parts of the plot could be distinguished (Fig. 3), as they are related to the progressing deformation of the specimen. Hence, the specimen presents an elastic linear behavior at (1). The higher slope for three infiltrations can be explained by the higher stiffness due to the additional infiltrations. In part (2), the torque applied is high enough to start the propagation of pre-existing defects (cf. Fig. 1). As a consequence, a change of the curve slope is observed. As the cross section is further twisted, the specimen starts to fail in part (3). Due to the densified interface, the material with three infiltrations can bear higher shear stresses before failing.

However, the energy is not sufficient to completely separate the specimen, presumably because some cracks are deviating from their initial plane leaving behind undamaged fiber bundles which act as crack bridges. The additional energy from further twist gradually enlarges the debonded area in part (4). Images of the fracture surface (Fig. 6) showed signs of delamination, and thus, fiber-matrix debonding was considered to be the predominant fracture mechanism.

To validate the set-up proposed, results were compared to standard methods. Fig. 9 shows the comparison of shear strength measured by the three methods used. The DNC test presents the lowest strength of all methods for both materials and, at the same time, shows the highest scatter. In contrast, results from SBB tests are the highest and show a minimum of scatter. Results obtained by torsion tests are in between the two standard methods, and presented moderate scatter. For a direct comparison of the test methods it should be noted that only torsion and DNC specimens showed clear interlaminar shear failure, e.g. as a result of delamination, whereas SBB specimen did not fail as would be expected from the assumed stress distribution. SBB should then be restricted to quality control tests, since failure occurs, in many cases, due to flexure and/or indentation of the supporting rolls [23].
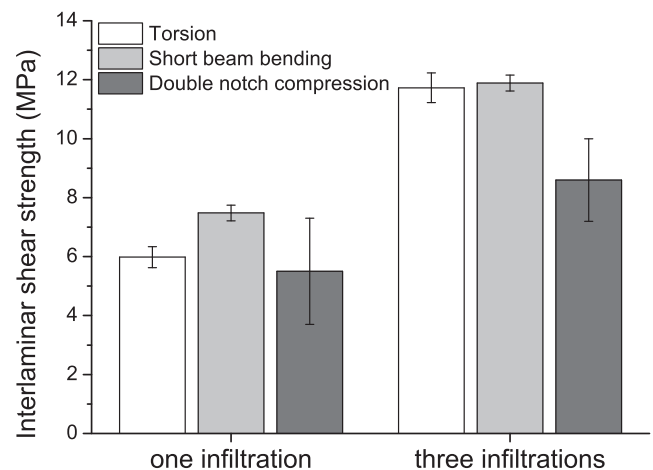


**Fig. 9:** Results obtained by the torsion tests without superimposed normal stresses in comparison with results from short-beam bending tests and double-notched compression tests.

Comparing torsion and DNC tests, it can be seen that the results are similar for samples with one infiltration, but quite different for three infiltrations. This difference can be explained by the enhanced notch sensitivity of three infiltrations specimens compared to the ones infiltrated once, thereby increasing the stress concentrations near to the notches of DNC specimens [4]. As the material densifies, stress concentrations around the notches are then more likely to affect the shear plane. In such cases, it can be presumed that the measured shear stresses tend to be lower, i.e. the strength of the material is underestimated. Given these facts, the denomination "interlaminar shear strength" always has to be linked to the test method used, which is referenced in most publications. However, an explanation of the fracture pattern should also be given to es-

timate the validity of the results, which is sometimes lacking.

Using the current setup, a state of pure shear stress can be achieved. The torsion specimen provides a gradient of shear stress through the reduced circular section with a maximum in the outer perimeter and zero stress at the center of the sample. Even if the different elastic properties of plies and inter-ply interface do not allow for the stress gradient to be continuous, these maxima/minima still remain. As seen in Fig. 5, the results from through-thickness tensile strength, using square specimens without the reduced section, are in the same range as those of the torsion tests with superimposed tensile tests, using specimens with a reduced cross-section. This indicates that the reduced section did not result in a reduction of the measured strength as a result of stress concentrations at the tip of the machined notch, but that the interlaminar strength is then rather determined by the amount and size of inter-ply defects surpassing any suspected effects of the sample geometry.

Another advantage of torsion tests is in regard to its simplicity. The test rig necessary for this technique can be easily found in most laboratories. Specimen preparation proved to be easy and requires little material for a big sample size. These advantages are crucial for the characterization of new composite materials. CMCs can be rather heterogeneous, and the process expenses are quite high. Therefore, usually only small plates are produced for characterization purposes during the development steps. Given the smaller size of the torsion specimen in comparison with other standard methods, several analyses can be performed with a limited amount of material, including the possibility of analyzing the material under biaxial conditions.

### (2)  Biaxial behavior

The application of superimposed normal stresses resulted in changes of the applicable shear stresses as shown in Fig. 4. Shear strength decreased with tensile loads and increased with compression loads. The different failure patterns of the material with three infiltrations are summa-

rized in Fig. 10. Debonding at the fiber-matrix interface was identified as the predominant failure mechanism for shear tests (cf. Fig. 6). The same aspect was identified when overlaying tensile stresses were applied (Fig. 10a). Given that both stresses act in the direction of separating the fiber plies, the predominant parameters are then the bonding strength between fiber and matrix, as well as the amount of pre-induced interlaminar defects and the grade of matrix filling. The suppression of interface cracks (Fig. 7b) by increasing compression leads to an increase of the fracture stress (Fig. 10b). Since the compression load presses the fiber plies together, signs of matrix damage are found at the regions of delamination-like fiber imprints. This is supported by significantly reduced load drops after the maximum stress has been passed. A different fracture mechanism is present at very high compressive stresses around the maximum in Fig. 5. In this case, matrix cracking takes place at the bridges between the fibers (Fig. 10c). The severe destruction of the matrix shown in Fig. 8 is enabled by the glassy state of the carbon that results from production. As for other vitreous materials, minimal deformation is induced by the compressive stress, yet beyond the point of fracture, cracks spread rapidly. If the compressive stress is too high, matrix cracking occurs to such an extent that the shear stress upon failure decreases as seen in the measured failure envelope (Fig. 5). Under these high stresses, the predominant parameter is the strength of the matrix.

The newly developed torsion test proved to be versatile as it is able to effectively control the level of superimposed normal stresses. For this purpose, other methods like slant or Arcan tests are difficult to apply in the case of CMCs. Under the biaxial conditions presented, fracture is no longer to be categorized as shear, tensile or compressive failure and the fracture patterns reflect the combined effects of superimposed stresses. In heterogeneous materials such as C/C, stresses and strains are diversely distributed between fiber and matrix and as normal and shear stresses are applied to a macroscopic specimen, both forms of stresses will interact on the microscopic level leading to the specific fracture phenomena as described.
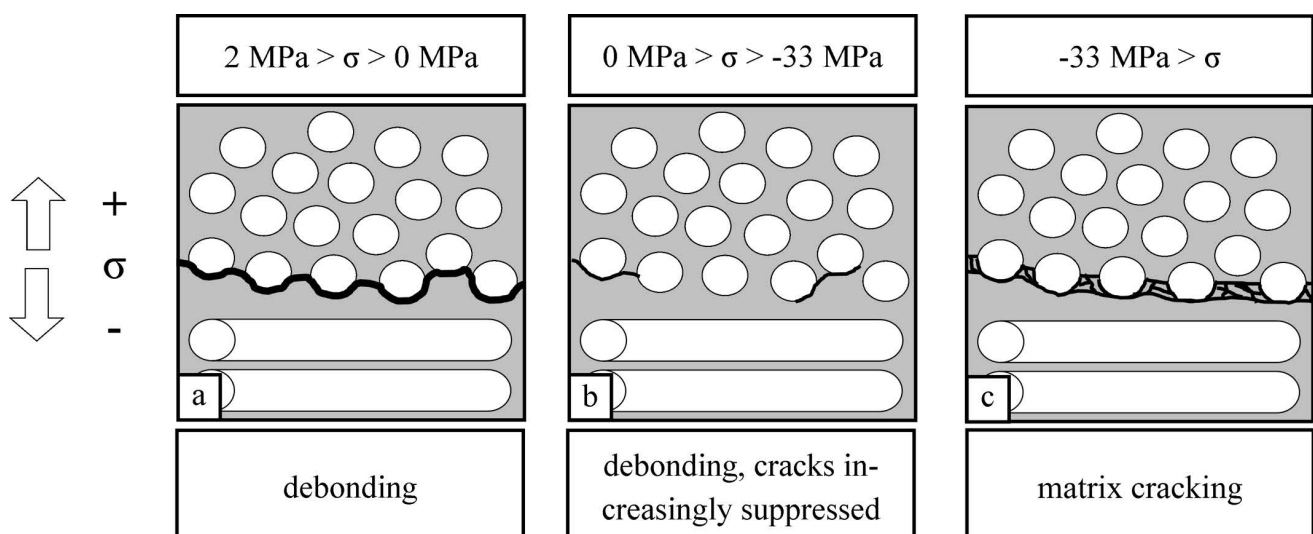


**Fig. 10:** Schematic view of interfacial region between fibers in 0° and 90° direction. Fracture patterns depending on the normal stress applied to the torsion samples are shown for the carbon/carbon composite with three infiltrations. Three models (a, b, c), with distinct stress ranges following the results in Fig. 5, are suggested.

## V. Conclusions

A new torsion test has been established to examine the interlaminar shear strength of ceramic matrix composites with different porosities. Test set-up and specimen preparation are simple. Normal stresses acting on the cross-section of the sample can be applied and well controlled, unlike with other standard methods like the short-beam bending test and the double-notched compression test. Since the fracture processes can be studied as they are localized in the designated area of the torsion samples the fracture patterns could be identified and related to the actual stress ranges.

Superimposed tensile stresses drastically reduce the shear strength of the material, whereas compression loads increase the shear strength up to a maximum beyond which a reduction of the shear stress at failure is observed. Different failure mechanisms are identified depending on the overlaying stresses. At tensile and low compressive stresses, delamination is the main factor. For increasing compressive loads, the formation of cracks is suppressed followed by shearing off the supporting matrix under high normal loads. The torsion test is thus able to allow for tests with and without superimposed normal stresses and to identify different interlaminar shear fracture mechanisms which cannot be discovered with any of the standard methods.

## Acknowledgement

## References

[1] Whitney, J., Browning, C.: On short-beam shear tests for composite materials, *Exp. Mech.*, **25**, 294–300, (1985).

[2] Casal, E., Granda, M., Bermejo, J., Bonhomme, J., Menéndez, R.: Influence of porosity on the apparent interlaminar shear strength of pitch-based unidirectional C-C composites, *Carbon*, **39**, 73–82, (2001).

[3] Fang, N.J.J., Chou, T.-W.: Characterization of interlaminar shear strength of ceramic matrix composites, *J. Am. Ceram. Soc.*, **76**, 2539–2548, (1993).

[4] Ünal, Ö., Bansal, N.P.: In-plane and interlaminar shear strength of a unidirectional Hi-nicalon fiber-reinforced celsian matrix composite, *Ceram. Int.*, **28**, 527–540, (2002).

[5] Thielicke, B.: Determination of interlaminar shear strength of carbon-fibre-reinformed carbons with the compression-shear test in the temperature range between room temperature and 2000 °C, in German, PhD thesis, Universität Karlsruhe, (1997).

[6] Li, M., Matsuyama, R., Sakai, M.: Interlaminar shear strength of C/C-composites: The dependence on test methods, *Carbon*, **37**, 1749–1757, (1999).

[7] Melin, L.N., Neumeister, J.M.: Measuring constitutive shear behavior of orthotropic composites and evaluation of the modified iosipescu test, *Compos. Struct.*, **76**, 106–115, (2006).

[8] Shi, Y., Tushtev, K., Koch, D.: Characterization of mechanical properties under shear load of a short-carbon-Fiber-reinforced C/SiC ceramic, *J. Ceram. Sci. Technol.*, **6**, 183–190, (2015).

[9] Hahn, L., Ansorge, F., Bruckner-Foit, A.: Damage and failure behaviour of a woven C/SiC material, *J. Mater. Sci.*, **32**, 5467–5475, (1997).

[10] Arcan, M., Hashin, Z., Voloshin, A.: A method to produce uniform plane-stress states with applications to fiber-reinforced materials, *Exp. Mech.*, **18**, 141–146, (1978).

[11] Gan, K.W., Laux, T., Taher, S.T., Dulieu-Barton, J.M., Thomsen, O.T.: A novel fixture for determining the tension/compression-shear failure envelope of multidirectional composite laminates, *Compos. Struct.*, **184**, 662–673, (2018).

[12] Ferraris, M., Ventrella, A., Salvo, M., Avalle, M., Pavia, F., Martin, E.: Comparison of shear strength tests on AV119 epoxy-joined carbon/carbon composites, *Compos. Part B-Eng.*, **41**, 182–191, (2010).

[13] Ventrella, A., Salvo, M., Avalle, M., Ferraris, M.: Comparison of shear strength tests on AV119 epoxy-joined ceramics, *J. Mater. Sci.*, **45**, 4401–4405, (2010).

[14] Ferraris, M., Ventrella, A., Salvo, M., Gross, D.: Shear Strength Measurement of AV119 Epoxy-Joined SiC by Different Torsion Tests, *Int. J. Appl. Ceram. Tec.*, **11**, 394–401, (2014).

[15] Greven, B.C., Gross-Barsnick, S., Koppitz, T., *et al.*: Torsional shear strength of novel glass-ceramic composite sealants for solid oxide fuel cell stacks, *Int. J. Appl. Ceram. Tec.*, **15**, 286–295, (2018).

[16] Kawai, N., Kotani, T., Kakimoto, Y., Sato, E.: Fracture behavior of silicon nitride ceramics under combined compression-torsion stresses analyzed by multiaxial fracture statistics, *J. Eur. Ceram. Soc.*, **31**, 1827–1833, (2011).

[17] Nohut, S., Usbeck, A., Özcoban, H., Krause, D., Schneider, G.A.: Determination of the multiaxial failure criteria for alumina ceramics under tension-torsion test, *J. Eur. Ceram. Soc.*, **30**, 3339–3349, (2010).

[18] Olsson, R.: A survey of test methods for multiaxial and out-of-plane strength of composite laminates, *Compos. Sci. Technol.*, **71**, 773–783, (2011).

[19] Aoki, T., Ogasawara, T., Ishikawa, T.: Effects of normal stress on the off-axis mechanical behavior of a plain-woven C/C composite, *Adv. Compos. Mater.*, **12**, 123–137, (2003).

[20] Goldberg, R.K., Carney, K.S.: Modeling the nonlinear, strain rate dependent deformation of woven ceramic matrix composites with hydrostatic stress effects included. In: Proceedings of the Eighth International LS-DYNA Users Conference, 2004.

[21] Bernachy-Barbe, F., Gelebart, L., Bornert, M., Crepin, J., Sauder, C.: Anisotropic damage behavior of SiC/SiC composite tubes: multiaxial testing and damage characterization, *Compos. Part A – Appl. Sci.*, **76**, 281–288, (2015).

[22] Shapovalov, K., Jacobsen, G.M., Alva, L., Truesdale, N., Deck, C.P., Huang, X.Y.: Strength of $SiC_f$-$SiC_m$ composite tube under uniaxial and multiaxial loading, *J. Nucl. Mater.*, **500**, 280–294, (2018).

[23] Abali, F., Pora, A., Shivakumar, K.: Modified short beam shear test for measurement of interlaminar shear strength of composites, *J. Compos. Mater.*, **37**, 453–464, (2003).